# Chloroplast Methyltransferase Homolog RMT2 is Involved in Photosystem I Biogenesis

*Rick G. Kim[a,b,1], Weichao Huang[a,1], Justin Findinier[a,1,2], Freddy Bunbury[a], Petra Redekop[a], Ruben Shrestha[a], Josep Vilarrasa-Blasi[b], Robert E. Jinkerson[c], Neda Fakhimi[a], Friedrich Fauser[a], Martin C. Jonikas[d], Masayuki Onishi[e], Shou-Ling Xu[a], and Arthur R. Grossman[a,b,2]*

[1]*R.G.K., W.H., and J.F. contributed equally to this work.*

[a]*Department of Biosphere Science and Engineering, Carnegie Institution for Science, Stanford, CA 94305, USA;* [b]*Department of Biology, Stanford University, Stanford, CA 94305, USA;* [c]*Department of Chemical and Environmental Engineering, University of California, Riverside, CA 92521, USA;* [d]*Department of Molecular Biology, Princeton University, Princeton, NJ 08540, USA;* [e]*Department of Biology, Duke University, Durham, NC 27708, USA*

[2]Corresponding Author:

Name: Justin Findinier and Arthur Grossman

Address: The Carnegie Institution for Science,

260 Panama St., Stanford, CA 94305

Email: jfindinier@carnegiescience.edu

agrossman@carnegiescience.edu

Tel: 650-325-1521

*Keywords*: photosynthesis, methylation, pyrenoids, oxygen sensitivity

## Abstract

Oxygen ($O_2$), a dominant element in the atmosphere and an essential molecule for most life on Earth, is produced by the photosynthetic oxidation of water. However, metabolic activity can cause the generation of reactive $O_2$ species (ROS) that can damage lipids, proteins, nucleic acids, and threaten cell viability. To identify and characterize mechanisms that allow cells to cope with the potentially negative effects of $O_2$ reactivity, we performed a high-throughput $O_2$ sensitivity screen on a genome-wide insertional mutant library of the unicellular alga *Chlamydomonas reinhardtii*. This screen led to the identification of several genes that, when disrupted, alter the cell's sensitivity to $O_2$ in the light. One of these genes encodes a protein designated Rubisco methyltransferase 2 (RMT2). Although this protein has homology to methyltransferases, it has not yet been demonstrated to catalyze methyltransferase reactions. Furthermore, the *rmt2* mutant has not been observed to be compromised for the level of Rubisco (first enzyme of Calvin-Benson Cycle; CBC), although the mutant cells were light sensitive, which is reflected by a marked decrease in the level of photosystem I (PSI), with much less of an impact on the other photosynthetic complexes; this mutant also shows upregulation of genes encoding the Ycf3 and Ycf4 proteins, which are associated with the biogenesis of PSI. The RMT2 protein has a chloroplast targeting sequence predicted by PredAlgo and PB-Chlamy[1,2], and rescue of the mutant with a wild-type (WT) copy of the gene fused to the mNeonGreen fluorophore indicates that the protein is within the chloroplast and appears to be enriched in/around the pyrenoid (an intrachloroplast compartment, potentially hypoxic, that is found in many algae that contain the $CO_2$-fixing enzyme Rubisco), but we also observe it more dispersed throughout the stroma. These results suggest that RMT2 may serve an important role in the biogenesis of PSI and that PSI biogenesis may be enriched around or within the pyrenoid, which may reflect the impact of $O_2$/reactive $O_2$ species on the efficiency with which PSI can assemble.

## Significance Statement

A high-throughput genetic screen was used to identify $O_2$ sensitive mutants of *Chlamydomonas reinhardtii* (Chlamydomonas throughout) that experience elevated oxidative stress in the light

relative to WT cells. Identification of genes altered in these mutants offers opportunities to discover activities that **a**) protect photosynthetic cells from oxidative damage, **b**) are required for proper and rapid assembly of photosynthetic complexes, which would limit ROS production during the assembly process, and/or **c**) facilitate the repair of damaged cellular complexes. A mutant identified in this screen is null for the *RMT2* gene, which was previously described as encoding Rubisco methyltransferase. RMT2 appears to be critical for PSI accumulation/biogenesis and is enriched in the pyrenoid, a chloroplast localized compartment harboring much of the Chlamydomonas Rubisco, suggesting a potential role for this compartment in the biogenesis of photosynthetic complexes.

## Introduction

In oxygenic photosynthesis, electron transport is driven by two photosystems, photosystem I and photosystem II (PSI and PSII). PSI uses absorbed light energy to drive electron transfer from plastocyanin (or cytochrome *c6*) to ferredoxin. Although the structure of PSI has been established at high resolution [3–8], there are still gaps in our knowledge of the steps involved in PSI biogenesis [9–13]. Detailing PSI biogenesis has been challenging because PSI assembly is rapid, making it difficult to identify assembly intermediates [9,10,14], and the core subunits of PSI (PsaA and PsaB) constitute approximately 80% of the total molecular mass of the holocomplex. Rapid PSI assembly is considered essential as intermediate assembly products may generate reactive species that chemically modify and damage intracellular structures and activities [14]. In addition, the rapid assembly of PSI may limit damage to certain prosthetic groups critical for its function; e.g. the three 4Fe-4S clusters of PSI are highly sensitive to $O_2$ [15–17]. Although $O_2$ sensitive constituents of PSI may be protected from damage within the assembled holocomplex, they would likely become susceptible to damage as a consequence of the accumulation of reactive oxygen species (ROS) that are generated in the process of assembling the complex. CGL71, one of the nuclear-encoded factors required for normal PSI assembly, has been implicated in protecting assembly processes from oxidative disruption [11].

To identify proteins involved in protecting the cells from $O_2$ reactivity or that result in $O_2$ sensitivity when they are absent/aberrant, especially in the light when the internal concentration of $O_2$ may be elevated, we performed a screen to identify $O_2$-sensitive mutants of the unicellular photosynthetic eukaryote, *Chlamydomonas reinhardtii* (Chlamydomonas throughout). We used the entire population of mutants in the CLiP (Chlamydomonas mutant Library Project) mutant library [18,19] to perform a large-scale screen for $O_2$ sensitive mutants. These mutants have unique built-in DNA barcodes that enable the use of deep sequencing for high-throughput quantification of the growth of each mutant in the library under different environmental conditions [19]; in this case, under different light and oxic conditions (**Fig. S1**). This screen identified more than a thousand mutants potentially hypersensitive to ambient $O_2$ levels relative to the WT, parental cells (**Fig. 1**).

Two highly $O_2$ sensitive mutants identified in this screen were disrupted for the gene encoding a protein homologous to Rubisco methyltransferase 2 (RMT2), which is thought to be involved in protein methylation, although this 'RMT-like' protein does not have all the typical features associated with methyltransferase activity. Post-translational modifications (PTM), including methylation of both histone and nonhistone proteins, play functional, regulatory, and structural roles in a range of organisms [20,21]. Advances in high-performance mass-spectrometry (MS) and quantitative proteomic approaches have enabled in-depth analyses of the association of PTMs with proteins integral to photosynthetic function [22–25]. The high sensitivity of *rmt2* mutants to $O_2$ damage suggests that the activity of RMT2, potentially methylation, can markedly impact processes that generate ROS, ameliorate potential damage by ROS, or participate in repair once damage occurs. Our additional analyses of the *rmt2* mutant suggest that it is aberrant for photosynthetic electron transport and is especially deficient in PSI, which generally leads to elevated levels of ROS in the light, causing phototoxicity [26,27].

## Results

**Oxygen sensitivity screen identified *rmt2* mutants**: To screen for Chlamydomonas mutants sensitive to $O_2$, we grew all mutants of the CLiP library as individual colonies on agar plates, transferred them from the agar to liquid medium to generate a full library mutant pool, and then divided the pool for growth under oxic and hypoxic conditions in both low light (LL) and high light (HL) (protocol in **Fig. S1**). The $O_2$ sensitivity of each mutant was individually assessed based on quantification of the number of barcoded reads representing each mutant in the library during growth in the dark and after transferring the cells to various growth conditions [19]; each barcode is unique to a specific mutant. Growth differences for each mutant are presented as a fold change under hypoxic relative to oxic conditions following growth for 7 generations at a light intensity of 300 µmol photons $m^{-2}$ $s^{-1}$ (**Fig. 1**). Strains mutated for the *RMT2* gene (Cre12.g524500) exhibited some of the highest $O_2$ sensitivity scores among those mutants that exhibited high confidence differences (based on p-values) in their growth rates (see **Materials and Methods**) under hypoxic relative to oxic conditions. Additional genes associated with $O_2$ sensitivity identified in the screen included RAT2 (Cre09.g388372; required for psaA RNA trans-splicing), a carlactone synthase (Cre02.g073900; a beta carotene dioxygenase, potentially involved in strigolactone synthesis) and a GreenCut protein CTP2 (Cre10.g424775; possibly required for SOD function in the chloroplast)(**Fig. 1**) [28]. Genes with mutants confidently showing $O_2$ sensitivity are listed in **Table S1**.

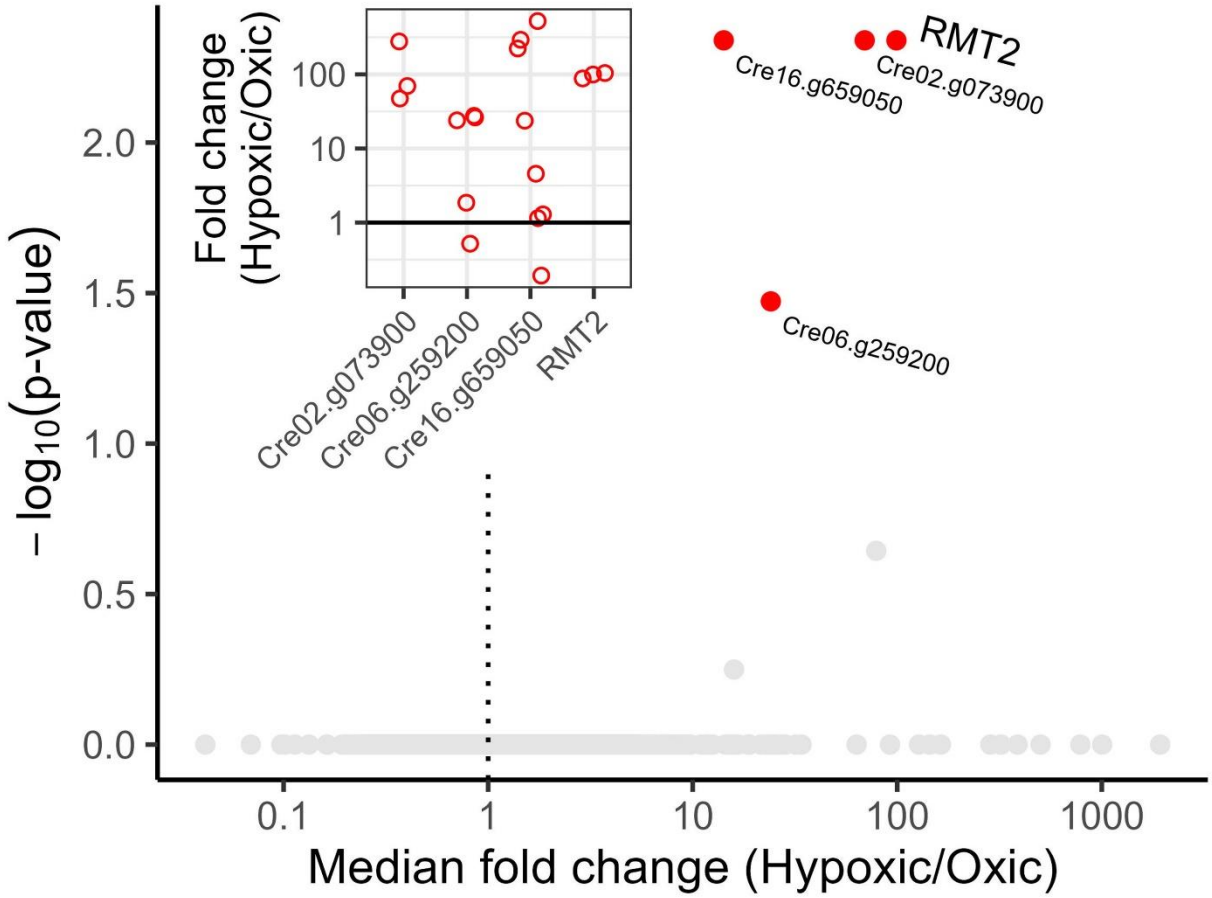


**Figure 1. Several Chlamydomonas mutants survive better under hypoxic vs oxic conditions, indicating potential genetic contributions to oxygen tolerance.** Based on the barcode sequencing results, each barcode in the sample was assigned read counts. Several criteria were applied, sequentially, to filter the initial data counts: insertions must be in 5' UTR, CDS, or intron regions of the gene; the insertion confidence level, defined in the initial analysis of the CLiP library and recorded in the description of each mutant (https://www.chlamylibrary.org/allMutants), must be 4 or below; the mean of the counts from the three initial replicates must be greater than 10, and similarly, the average of the final counts under the hypoxic and oxic conditions must be greater than 10; mutants must only have one barcode representing a single mutant gene; the number of mutant alleles per gene must be 2 or more. The approach for calculating whether genes had a statistically significant role in oxygen tolerance was similar to Li et al. 2019. A threshold to define a mutant as having an oxygen-sensitive phenotype was set at 10 times higher counts+1 in the hypoxic high light vs oxic high light screen. For each gene, a p-value was generated using Fisher's exact test comparing the numbers of alleles in that gene with and without a phenotype to the numbers of all insertions in the screen with and without a phenotype. A false discovery rate correction of the p-values was performed using the Benjamini-Hochberg (BH) procedure. The x-axis represents the median fold-difference in mutant counts+1 between hypoxic and oxic conditions for all mutants mapping to a gene. The y-axis represents the BH-adjusted p-value. The points highlighted in red have an adjusted p-value<0.05 and are plotted in the top-left inset, which shows the fold-change in abundance of each of their mutant alleles.

In the two Chlamydomonas *rmt2* mutants, *rmt2-1* (CLiP catalog number: LMJ.RY0402.237082) and *rmt2-2* (LMJ.RY0402.255338), identified in this screen, the *AphVIII* gene (paromomycin resistance) was inserted into the 4th intron (*rmt2-1*) and 9th exon (*rmt2-2*) (**Fig. 2A**). These insertions likely resulted in a loss of gene function based on the phenotype of the mutants and the ability to rescue the mutant phenotypes by ectopic expression of the wild-type (WT) *RMT2* gene (see below). RMT2 has a predicted transit peptide as well as both a Rubisco Substrate Binding (RSB) domain (**Fig. 2B**, underlined in blue) and a SET domain (acronym from the Drosophila Trithorax protein [Su(var)3-9, Enhancer-of-zeste and Trithorax]) (**Fig. 2B**, underlined in red); the latter domain harbors the active site of the enzyme catalyzing the transfer of methyl groups from S-adenosyl-L-methionine (AdoMet) to the amino group of protein lysine residues, including those of histones [29]. RMT2 also has homologs in *Pisum sativum*, *Spinacia oleracea*, and *Arabidopsis thaliana*, as shown in the Clustal Omega alignment of RMT2 homologs (**Fig. 2B**). Furthermore, Chlamydomonas has four other genes encoding proteins with significant homology to RMT2 (RMT1, RMT3-5). Examination of the sequences of these RMT homologs indicates that some of these proteins have the SET domain with the NHS motif which is involved in AdoMet binding, as well as the specific catalytic tyrosine common to methyltransferase proteins of the RMT family [30]. However, although RMT2 has a SET domain, this domain is missing the NHS motif and the catalytic tyrosine residue, although it does have a tyrosine that could potentially function in catalysis that is 9 amino acids upstream of the position of the catalytic tyrosine in other proteins of this family.

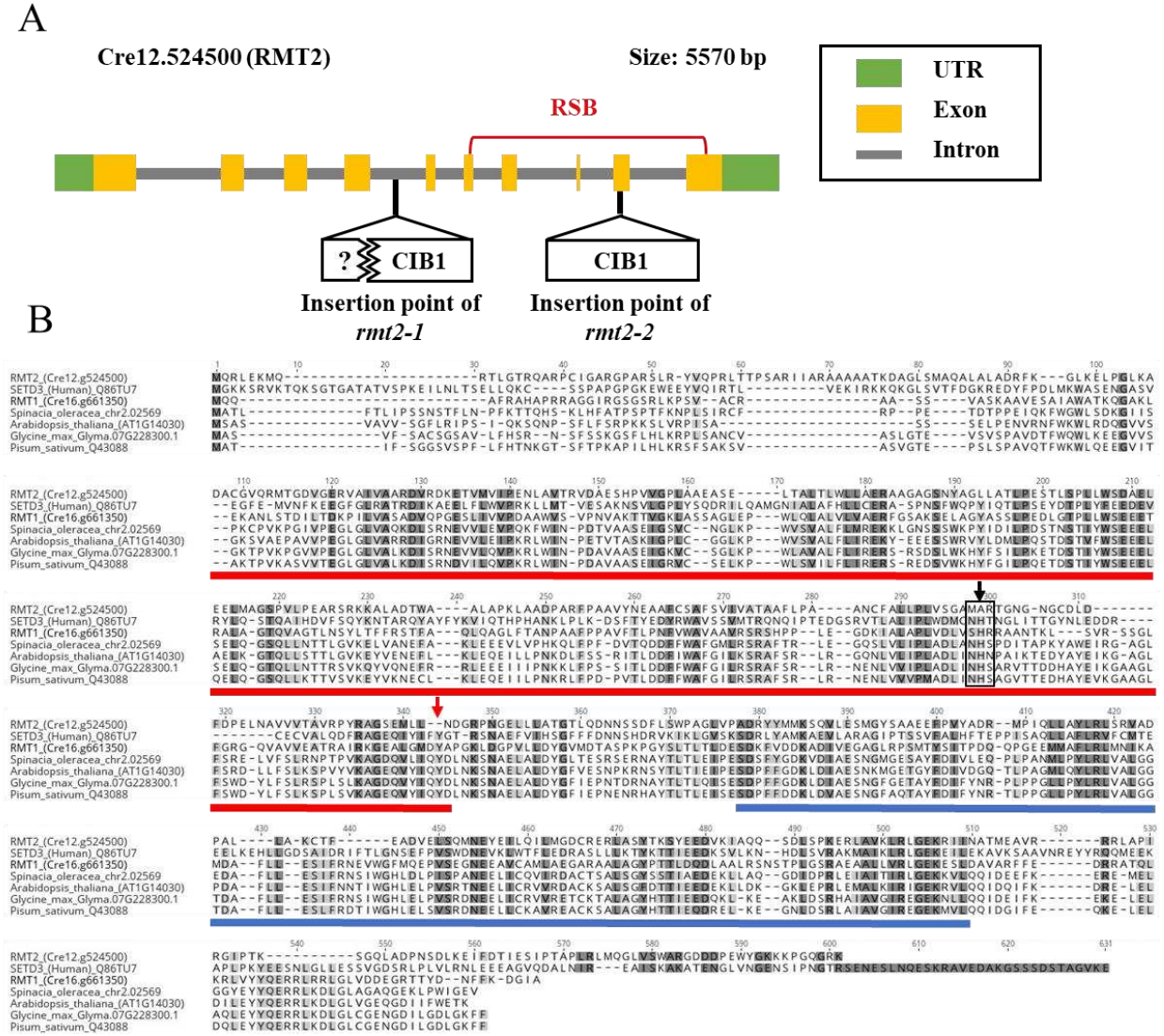


**Figure 2. Positions of insertions in *rmt2* mutants, and RMT2 homologue sequence alignments.** (A) *RMT2* gene showing position of inserted CIB1 cassette that includes *AphVIII* gene. Exons are yellow rectangles, introns grey lines, and 5'- and 3'-UTRs green rectangles. CIB1 is inserted into the 4th intron and 9th exon in the same and opposite orientation as the *RMT2* gene in *rmt2-1* and *rmt2-2* mutants, respectively. The junction sequences of the CIB1 insertion in *rmt2-2* were confirmed at both 5' and 3' ends. Only the 3' junction was confirmed in *rmt2-1*, however, the sequence upstream of the 5' end of *rmt2-1* 5' is intact (from 11 bp upstream of the insertion site). The RSB (Rubisco Substrate Binding) domain of RMT2 is indicated in a red bracket. (B) Clustal Omega alignment of RMT2 homologs from Spinacia oleracea, Arabidopsis thaliana, Glycine max, and Pisum sativum along with SETD3 from humans and RMT1 from Chlamydomonas. The SET domain based on the SETD3 sequence is underlined in red. The RSB domain, based on the RMT2 sequences, is underlined in blue. The conserved residues are highlighted in dark grey (identical for all) and light grey (conserved for all). The NHS motif and the catalytic tyrosine residue of the SET domain in SETD3 are indicated by a black and red arrow, respectively.

**The *rmt2* mutant is high light sensitive and rescued by hypoxic conditions:** Since *rmt2* mutants exhibited high $O_2$ sensitivity based on our initial screen, they were expected to show improved survival under hypoxic conditions. Growth studies demonstrated that *rmt2-1* was unable to grow under oxic, HL conditions (in this case 750 µmol photons $m^{-2}$ $s^{-1}$), but its growth was similar to that of WT cells under hypoxic, HL conditions (**Fig. 3A**). Furthermore, growth of the mutant occurred under oxic conditions if the light intensity during growth was low; once the intensity was raised above 50 µmol photons $m^{-2}$ $s^{-1}$ the cells stopped growing and lost viability (**Fig. S2**). This growth phenotype was rescued by ectopic expression of a WT *RMT2* gene in the *rmt2-2* mutant (**Fig. 3A**). These results demonstrate that both light and $O_2$ levels strongly impact growth and viability of the mutant, raising the possibility that an aberration in photosynthetic processes in the mutant is responsible for the $O_2$ sensitive phenotype.

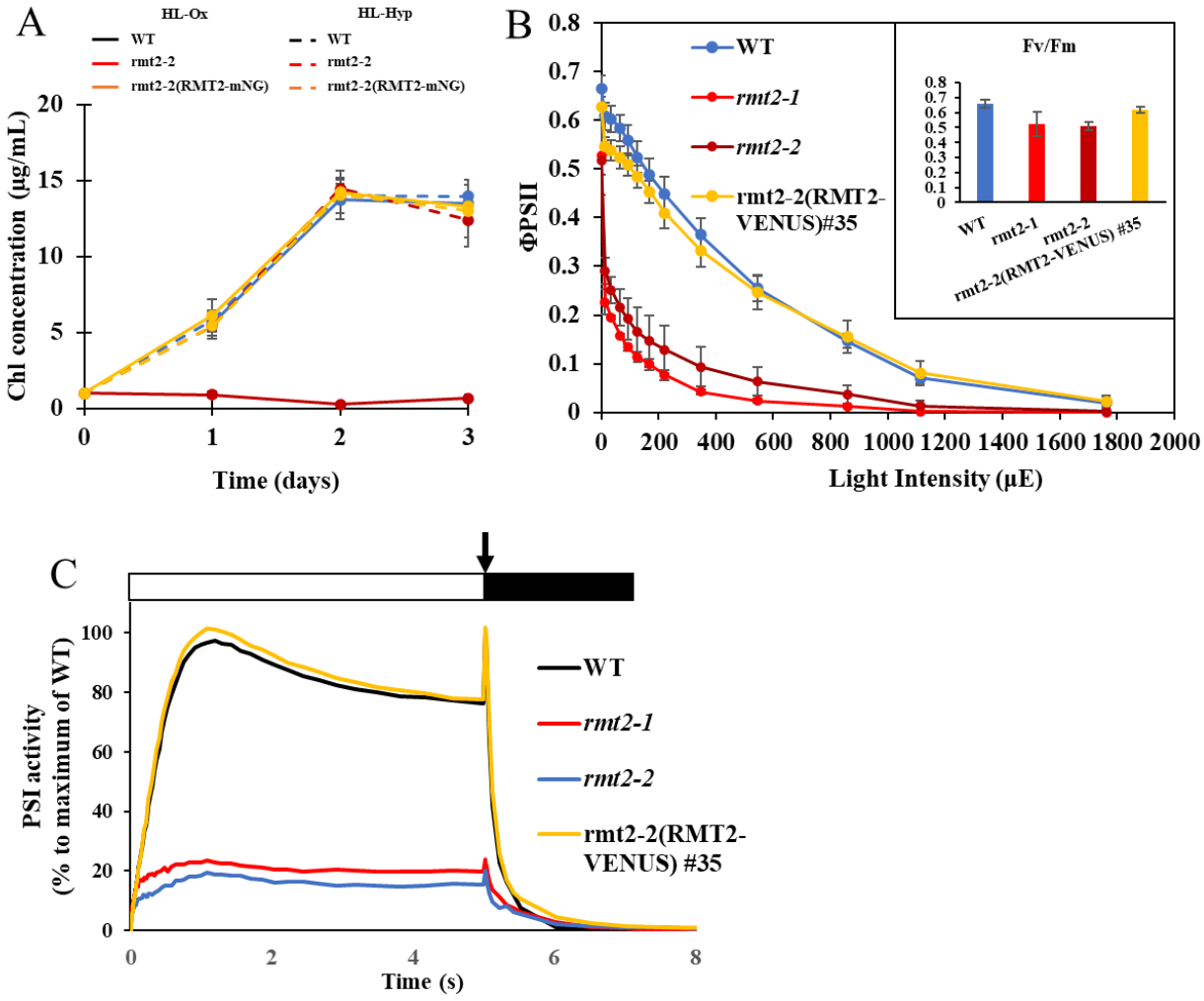


**Figure 3. *rmt2* mutants are sensitive to oxygen and have aberrant photosynthesis. (A)** Growth of WT

and *rmt2-2* and rmt2-2(RMT2-mNG) under HL-Hy and HL-Ox conditions. WT, *rmt2-1* and rmt2-2(RMT2-mNG) cells were harvested during exponential growth in low light (30 µmol photons $m^{-2}$ $s^{-1}$) before inoculation into HL-Hy (750 µmol photons $m^{-2}$ $s^{-1}$; hypoxic gas*) and HL-Ox (750 µmol photons $m^{-2}$ $s^{-1}$; air) conditions. Cultures were bubbled with the indicated gas mixture at the flow rate of 500 mL $min^{-1}$ with constant agitation (350 rpm). Chl concentrations were measured and plotted over the course of 3 days. *Hypoxic gas: 10% Air balanced by 89.96% $N_2$ and 0.04% $CO_2$. (µE = µmol photons $m^{-2}$ $s^{-1}$) **(B)** Quantum yield of PSII based on the fluorescence parameter ΦPSII, (which is (Fm'−Fs)/Fm') in WT, *rmt2-1*, *rmt2-2*, and the rmt2-2(RMT2-VENUS) #35 rescued strains. Cells used for analyses were in exponential growth under low light (30 µmol photons $m^{-2}$ $s^{-1}$) oxic conditions. For measurements, samples were incubated in the dark for 30 min and exposed to 1 min of actinic light at the intensities indicated on the x axis. Values are the mean of three biological replicates, and error bars represent standard deviations. The inset shows the Fv/Fm of each of the samples. (**C)** P700 oxidation and reduction kinetics of WT, the *rmt2-1* mutant, and the complemented strain (rescued with WT *RMT2* fused to a Venus tag). Cells were grown under LL-Ox conditions. Absorbance differences were monitored at 705 nm and 740 nm during continuous illumination with 300 µmol photons $m^{-2}$ $s^{-1}$ for 5 sec (white box), followed by a saturating light pulse at 1500 µmol photons $m^{-2}$ $s^{-1}$ (arrow) and a 3 sec dark incubation (black box). WT and *rmt2-1* samples were concentrated to 30 µg chl $mL^{-1}$. DCMU (PSII inhibitors) was included at a concentration of 10 µM to block electron flow from PSII. Kinetics were normalized by setting the maximum point of WT as 100%. Values are mean of three biological replicates.

**Photosynthetic activities are compromised in *rmt2***: To identify the cause(s) of light and $O_2$ sensitivity, we characterized the photosynthetic activities of WT, the *rmt2-1* and *rmt2-2* mutants, and the *rmt2-2* rescued strains (using VENUS or mNeonGreen fluorophores). The allelic *rmt2* mutants both showed a marked reduction in ΦPSII relative to WT and the complemented cells at all light intensities, although the $F_V/F_M$ values of WT and the mutants were only slightly different (**Fig. 3B**). These findings suggest that PSII reaction center function in the mutant was not significantly compromised and that there is a lesion in photosynthetic electron transport downstream of PSII. Measurements of PSI activity in *rmt2-1* and *rmt2-2* revealed a reduction to 10-20% of the activity measured in WT and the complemented cells (**Fig. 3C**). This loss of PSI activity explains the diminished ΦPSII and HL sensitive phenotypes. Immunoblot analysis of polypeptides of the photosynthetic apparatus, presented in **Fig. 4**, show that both mutants are strongly deficient in the levels of all PSI polypeptides (shown are PsaA, PsaC, PSAD, and PSAH; normalized to tubulin abundance) after growth under LL conditions (30 µmol photons $m^{-2}$ $s^{-1}$). Levels of most polypeptide subunits of other photosynthetic complexes, including ATP synthase (AtpA), cyt $b_6f$ (PetA), PSII (PsbA and PSBB), and Rubisco (RbcL and RBCS), were not strongly impacted in the mutants (**Fig. 4**), although some decline in the levels of PsbA and PetA was

observed, suggesting that the function of RMT2 extends beyond the accumulation of PSI, or that the mutant may experience some damage that impacts the levels of the other complexes even in LL. This potential secondary effect of lower PSI on the overall levels of other photosynthetic proteins is also consistent with the LC-MS/MS results (**Fig. S3**). Interestingly, the chloroplast-encoded PSI assembly factors (Ycf3 and Ycf4) were significantly upregulated in both of the *rmt2* mutants (**Fig. 4**), raising the possibility that impaired PSI assembly in the mutants elicits a compensatory mechanism(s) that leads to elevated assembly factor levels, and/or that the cells accumulate more PSI assembly intermediates that maintain a more sustained association with assembly factors, allowing for their accumulation.

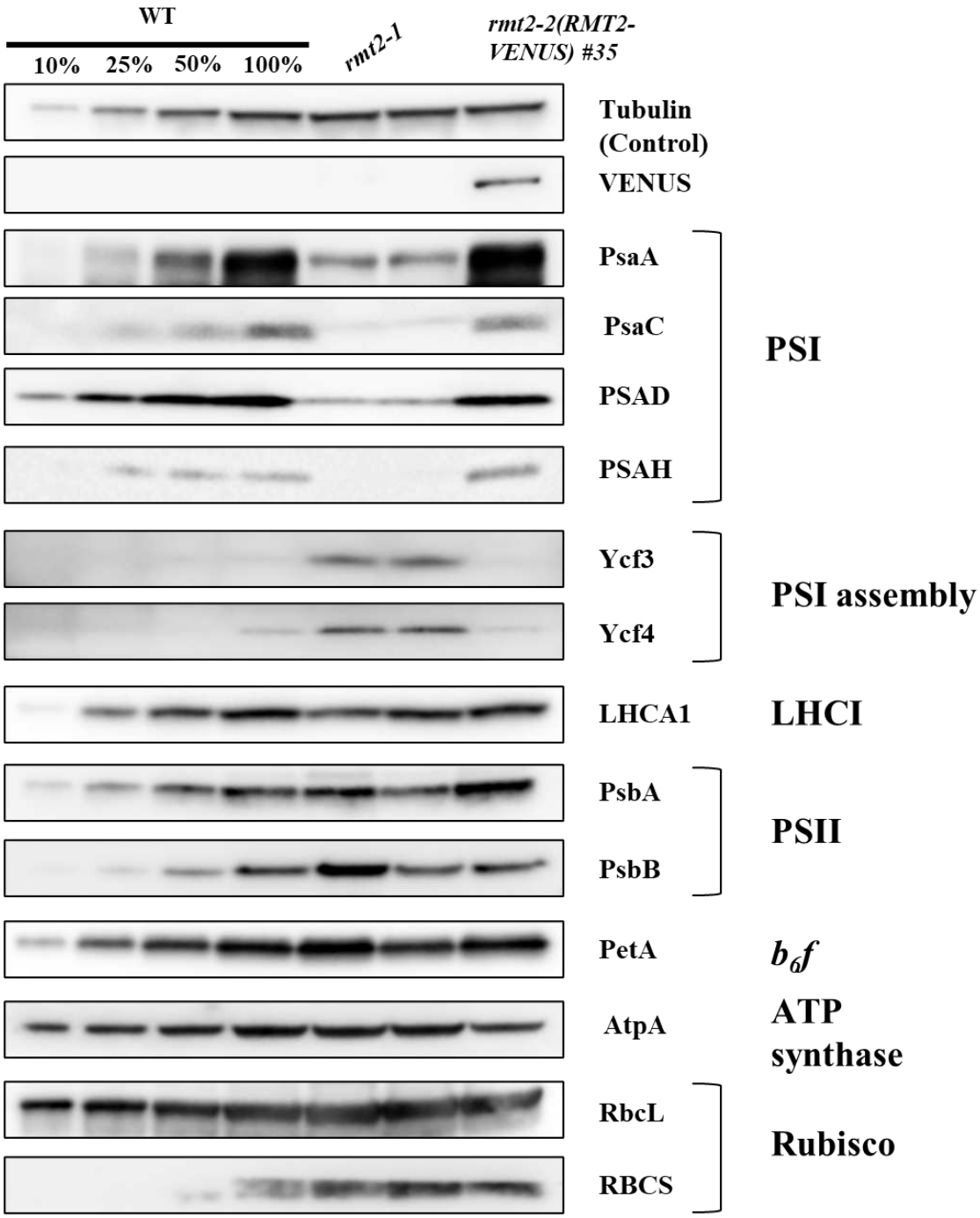


**Figure 4. Immunoblot analysis of polypeptides of photosynthetic complexes of WT and *rmt2* mutants.** Chlamydomonas proteins from WT, *rmt2-1* and *rmt2-2* grown under LL-Ox conditions were resolved by SDS-PAGE on a 12% polyacrylamide gel and detected immunologically. Antibodies used for the analysis were raised to polypeptides indicated on the right side of the figure. 1 µg of Chl was loaded for each sample analyzed by Western blots (except for the WT 10%, 25% and 50%, which were 0.1 µg, 0.25 µg and 0.5 µg, respectively).

**Impact of loss of RMT2 on protein profiles**: To quantify the overall impact of a loss of RMT2 on the levels of Chlamydomonas proteins, we performed quantitative proteomics on WT and the *rmt2-1* and *rmt2-2* mutants after labeling the cells with $^{15}N$ and $^{14}N$ ammonium (separate experiments were performed using heavy labeling of WT and *rmt2-1* and *rmt2-2* mutant cells) under LL oxic conditions. After labeling, total proteins from 'heavy' and 'light' samples (see **Materials and Methods**) were extracted from the WT and mutant cells and equal amounts of each sample, based on chlorophyll (chl) content, were combined, processed, and analyzed by mass spectrometry (**Fig. 5A**). We found 27 proteins, including HSP22F, DEG11, and FTSZ, that were elevated by at least 3-fold in the mutants relative to WT cells (**Table S2**). These proteins are associated with stress responses (protein folding and degradation) in Chlamydomonas. There were also 21 proteins that were at least 3-fold less abundant in the mutants relative to the wild type cells. Among them were many PSI-associated polypeptides, as expected from our physiological and immunological analyses, and some $CO_2$ concentrating mechanism (CCM)-related proteins (**Table S2**). However, the absence of RMT2 in the cells does not alter the induction of CCM-associated genes under low $CO_2$ conditions (**Fig. S4**) or the ability of the cells to maintain a prominent pyrenoid (**Fig. 6B**). The impact of RMT2 on the levels of CCM transcripts might be indirect and result from higher intracellular accumulation of $CO_2$ in the mutant during growth on acetate (which generates $CO_2$ when metabolized) because of its reduced photosynthetic activity and inability to efficiently fix $CO_2$ (the intracellular concentration of $CO_2$ would increase). This hypothesis is supported by the findings that this mutant shows reduced values for ΦPSII even at very low light intensities (**Fig. 3B**) and a marked reduction in PSI activity (**Fig. 3B**).

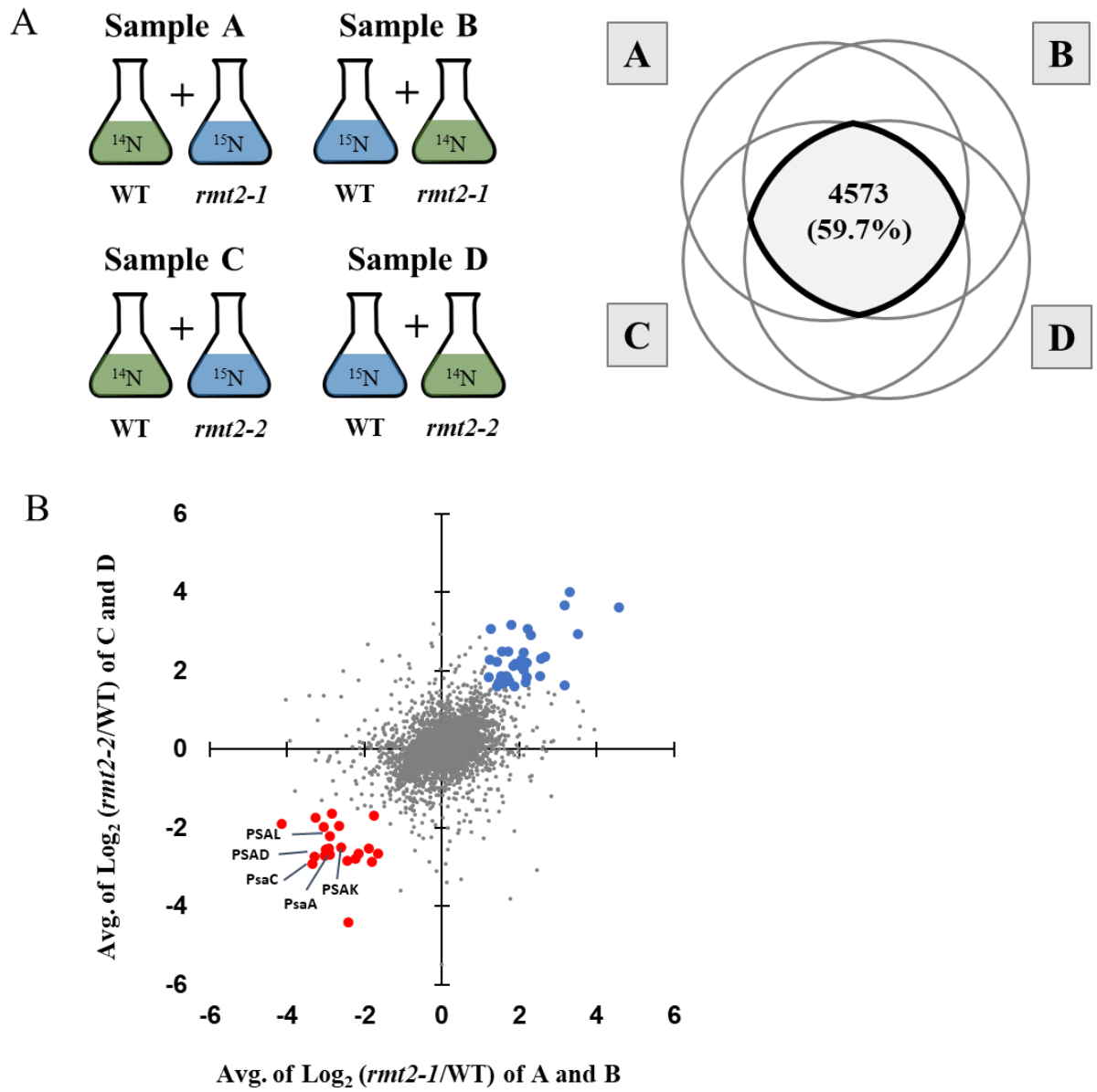


**Figure 5. Peptide identification by LC-MS/MS and correlation between reciprocal samples.** WT, *rmt2-1* and *rmt2-2* cells were reciprocally labelled with $^{15}$N-TAP medium. (A) Sample A contains $^{14}$N-WT and $^{15}$N-*rmt2-1*; Sample B contains $^{15}$N-WT and $^{14}$N-*rmt2-1*; Sample C contains $^{14}$N-WT and $^{15}$N-*rmt2-2*; and Sample D contains $^{15}$N-WT and $^{14}$N-*rmt2-2*. The 4 samples were analyzed separately by LC-MS/MS, and peptides derived from Chlamydomonas proteins were detected. Venn diagram showing 4573 proteins for which peptides were detected in all Samples A, B, C, and D. (B) Plot showing the correlation between the *rmt2-1* samples (Sample A and B) and the *rmt2-2* (Sample C and D). Dots represent log2 values of the median MS1 peak ratios of $^{15}$N/$^{14}$N (Sample A or C) or $^{14}$N/$^{15}$N (Sample B or D) among peptides of the same protein. 4573 data points were plotted. Those proteins with peptides that decreased by ≥3-fold in both *rmt2-1* and *rmt2-2* are highlighted in red, while those increased by ≥3-fold in both *rmt2-1* and *rmt2-2* are highlighted in blue. The remaining data points were marked as grey.

**PSI defect in *rmt2* mutants appears to be post-transcriptional:** To test if the low PSI accumulation in the *rmt2* mutant is a consequence of transcriptional regulation, we quantified transcript levels from both chloroplast and nuclear genes encoding subunits of PSI (*PsaA*, *PsaC*, *PSAD*, and *PSAE*) in *rmt2* and WT cells grown under LL oxic conditions (**Fig. S5**). The chloroplast-encoded PSI genes (*PsaA* and *PsaC*) have similar transcript levels in the two *rmt2* mutants relative to the WT and complemented cells, while the nucleus-encoded PSI transcript levels (*PSAD* and *PSAE*) may be affected slightly in one of the mutant alleles (*rmt2-1*). The level of RMT2 transcripts detected in both *rmt2* mutants was very low. Overall, the results suggest that the lack of RMT2 protein does not strongly impact the level of PSI transcripts and that the function of RMT2 in PSI accumulation is likely post-transcriptional.

We also investigated if the reduced accumulation of PSI subunits in the *rmt2* background was potentially due to their increased degradation rate (**Fig. S6**). In the presence of translation inhibitors, the PSI subunit PsaA showed similar stability in the *rmt2-2* strain as in the wild-type background (compare top panels) and the complemented strain (bottom panel), suggesting that the diminished level of PSI in the RMT2 deficient strains is likely related to protein synthesis or less efficient complex assembly. PsbA protein turnover was used as a control, showing that the presence of CAP and CHX resulted in a more rapid loss of PsbA protein in WT cells, *rmt2-2* mutant cells and the rescued strain (*rmt2-2* + RMT2-mNG) relative to the untreated sample.

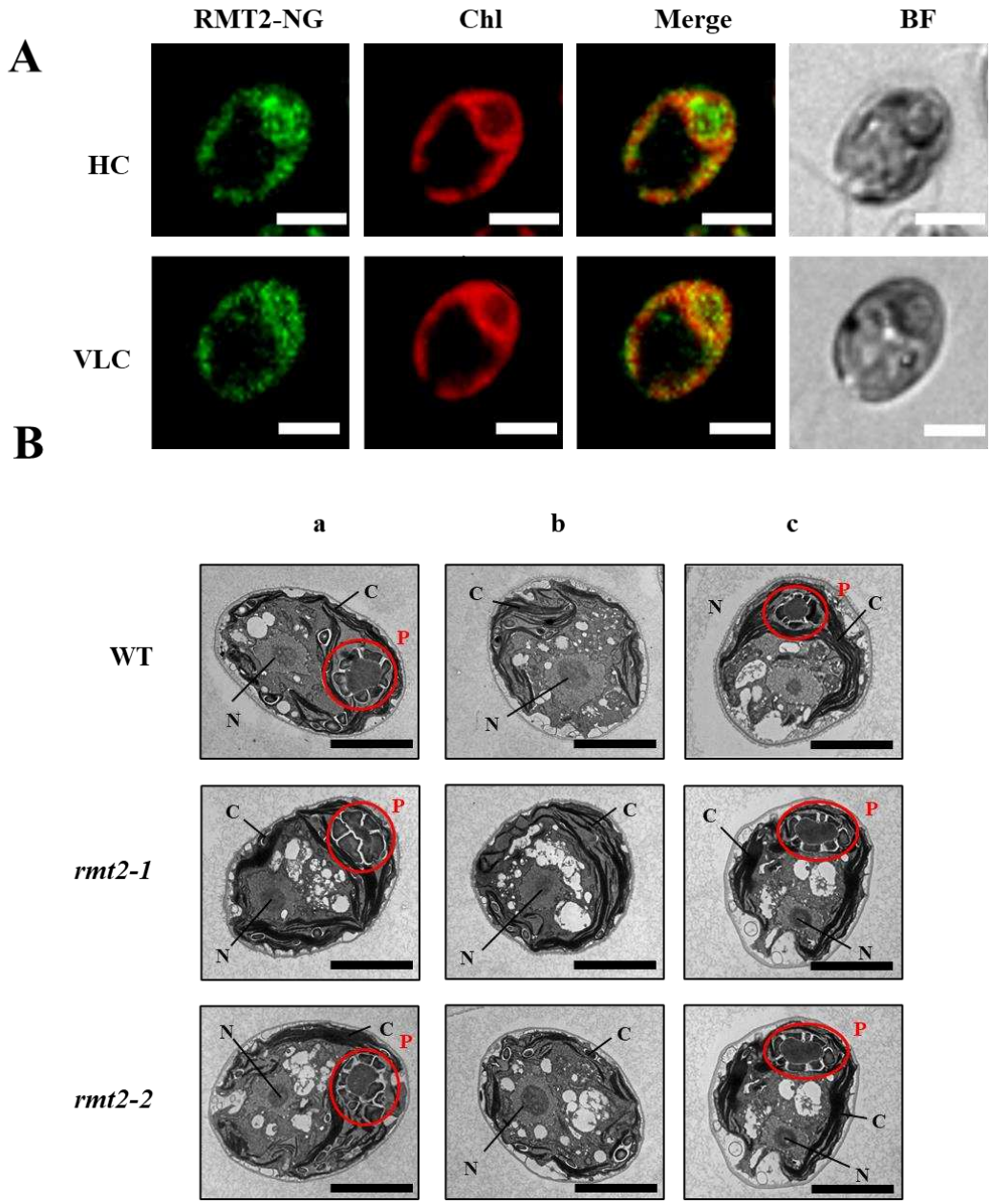


**Figure 6. Subcellular localization of RMT2 and pyrenoid structure in *rmt2* mutants. (A)** Localization of RMT2-mNG in high (HC, 3%) and very low (VLC, 4h at 0%) $CO_2$ conditions. Shown are RMT2-mNG (mNeon green) localization, Chlorophyll autofluorescence (Chl), merge of Neon green and chlorophyll fluorescence (Merge), brightfield (BF). Each image is a maximal projection of 10 cross sections from the cortex to the middle of the cells. Scale bar: 5 µm. **(B)** TEM of sections of WT, *rmt2-1* and *rmt2-2* cells. (a) Cells with pyrenoid structures (grown in TAP medium at 20 µmol photons $m^{-2}$ $s^{-1}$). (b) Cells without pyrenoid structures (grown in TAP medium at 20 µmol photons $m^{-2}$ $s^{-1}$). (c) Cells with pyrenoid structures (grown in HS medium at 50 µmol photons $m^{-2}$ $s^{-1}$). Pyrenoid structures are highlighted by red circles. N, nucleus; C, chloroplast; P, pyrenoid. Scale bar = 5 µm.

**RMT2 location under high and very low $CO_2$ conditions:** To help predict the function of RMT2, we also determined its subcellular location under high and very low $CO_2$. *RMT2* was fused to the

sequence encoding the mNeonGreen fluorophore (RMT2-mNeonGreen) and the fusion construct was introduced into the *rmt2-2* mutant background (see **Materials and Methods**). The *rmt2-2* mutant was rescued by the RMT2-mNeonGreen construct; the transformed strain was able to grow under both HC (3%) and very low $CO_2$ (VLC; <0.02% $CO_2$) conditions (in TP medium at 150 µmol photons $m^{-2}$ $s^{-1}$). At both of these $CO_2$ conditions, much of the fluorescence of the RMT2-mNeonGreen fusion protein was associated with the pyrenoid, although there was a substantial amount that was more generally distributed in the chloroplast stroma (**Fig. 6A** and **Fig. S7**). Both the presence of a transit peptide and the association of RMT2 with proteins of the chloroplast [23] already suggested its localization in the chloroplast. However, these results also raise the possibility that the association of RMT2 with the pyrenoid may be important for the biogenesis of photosynthetic complexes, especially PSI. Interestingly, the PSBP4 protein, which is involved in PSI assembly [31], also localizes around the pyrenoid as well as on pyrenoid tubules [2], which suggests that the assembly of PSI may occur both in the pyrenoid (or in close proximity to the pyrenoid) and in the chloroplast stroma, although some mis-localization of the gene product used for rescue may occur because of the bulky protein fluorophore and overexpression of the introduced *RMT2* gene. Additionally, RMT2 localization did not appear to be impacted by the level of $CO_2$ in the environment (**Fig. 6** and **Fig. S7**).

**Methylation of subunits of the photosynthetic apparatus**: To examine whether the PSI complex that accumulated in the *rmt2* mutants showed any aberrations of methylation of PSI subunits, we purified thylakoid membranes from WT, *rmt2-1* and *rmt2-2* and quantified the methylated peptides of the various PSI subunits (PSAD and PSAE). Methylated proteins are listed in **Table S3**. Only high confidence proteins are shown, although many methylation sites were potentially identified in more than 50 polypeptides. Hence, while many proteins of the photosynthetic complexes are methylated, there is no clear difference between WT cells and the *rmt2* mutants (**Fig. S8**).

## Discussion

We exploited the power of the CLiP library to simultaneously screen 58,101 mutants covering ~83% of the Chlamydomonas nuclear protein-coding genes to identify strains more sensitive to

oxidative conditions than the parental cells [18,19]. This analysis yielded a list of genes encoding proteins (**Fig. 1, Table S1**) that potentially allow Chlamydomonas to effectively cope with oxidative stress. The list includes CGL71, a protein previously shown to be required for protection of PSI assembly against oxidative damage [11]; these findings establish the feasibility of this screen. Furthermore, this list provides an opportunity for researchers to discover novel proteins involved in photoprotection, identify $O_2$ sensitive steps in assembly, and repair ROS damaged complexes.

RMT2 is a protein that strongly impacts PSI accumulation (**Fig 3** and **4**). The reduced level of PSI in the mutant appears to result in $O_2$ sensitivity (**Fig. 1** and **3**), similar to the phenotype observed for other PSI mutants [11,32,33]. The *rmt2* mutants exhibited reduced PSI activity in LL oxic and dark oxic conditions (**Fig. S9**), which reflects a marked reduction in the level of PSI subunits in these strains. These mutants die under HL oxic conditions but can be rescued (e.g. restores PSI activity, normal levels of PSI polypeptides, and growth under HL oxic conditions) when a WT copy of RMT2 is ectopically expressed in the mutant genetic background (**Fig. 3** and **4**). The mutant also grows well in HL under hypoxic conditions (**Fig. 3**), with PSI activity somewhat higher than under dark-oxic or LL-hypoxic conditions (**Fig. S9**); the activity can reach as much as ~ 40% of that of WT activity under the former conditions. These phenotypes are different from those of the *cgl71* mutant, which accumulates near normal levels of PSI in dark-hypoxic conditions and almost no PSI when maintained under the dark-oxic conditions [11]. Hence, oxidative stress in *cgl71* appears to inhibit PSI assembly in both the light and dark and this can be reversed when the cultures are made hypoxic. In contrast, in the *rmt2* mutant, PSI levels remain low in the dark, LL oxic and LL hypoxic conditions, with only some increase in the level under HL hypoxic conditions, suggesting that the defect in PSI accumulation is not impacted strongly by oxic conditions, but that growth and viability are impacted; hypoxia can facilitate growth of *rmt2* even under HL conditions, without restoring WT levels of PSI. Therefore, RMT2 and CGL71 likely function at different stages of the assembly process, which in turn leads to different phenotypes; while the lower levels of PSI in *cgl71* can be mostly reversed under hypoxic conditions, in *rmt2* the accumulation of PSI is markedly reduced even under hypoxic conditions, but the level of PSI that is maintained (15-20% under dark oxic and LL hypoxic and up to 40% under HL hypoxic conditions) allows the cells to grow as long as the $O_2$ levels remain low. Furthermore, we were unable to show any difference

in the turnover rate of PSI subunits in the *rmt2* mutant relative to WT cells, suggesting that the PSI complexes that form in the mutant cells are stable. Whereas PSI biogenesis is affected by $O_2$ in *cgl71* mutant (a tetratricopeptide repeat protein), possibly through protection of the PSI 4Fe-4S centers during assembly of the complex, as previously discussed [11], $O_2$ does not strongly impact the biogenesis/accumulation of PSI in *rmt2*, but it does markedly influence the growth and viability of the mutant cells, suggesting that the growth defect is a consequence of the damaging impact of ROS that is generated by the photosystems, and that ROS damage can be especially severe under HL conditions and when there is an imbalance in electron transport [34,35].

Trimethylation of the ε-amino group of Lys-14 of the large subunit of Rubisco of tobacco and muskmelon was demonstrated over three decades ago [36]. The enzyme associated with this modification was designated RMT (Rubisco methyltransferase), suggesting that the substrate of this enzyme may be the large subunit of Rubisco. The function of RMT2 was predicted based on homology to Rubisco LSMT (Large Subunit Methyl Transferase) proteins from various plant species, including *Pisum sativum* (pea), *Nicotiana rustica* (tobacco), *Spinacia oleracea* (spinach), and *Arabidopsis thaliana* (Arabidopsis). As shown in **Fig. 2**, RMT2 in Chlamydomonas is similar to the plant RMTs and paralogous sequences in Chlamydomonas, such as RMT1, which encodes a methyltransferase that appears to be involved in methylation of fructose-bisphosphate aldolase [37]. The RMT enzyme was initially purified and characterized from tobacco and pea [38–40]. For a few decades, it was one of a few non-histone lysine methyltransferases identified. Most homologous proteins in other organisms, including those identified in non-plant species, were also given the name Rubisco LSMT even though it was not established that the homologs functioned in methylation of the Rubisco large subunit. Interestingly, Lys-14 of the large subunit is conserved but not methylated in Chlamydomonas, spinach, or Arabidopsis [37,41,42]. Therefore, the large subunit of Rubisco is unlikely to be the substrate of LSMT proteins in Chlamydomonas, although RMT2 has an LSMT binding domain that may function in binding interacting partners. RMT type methyltransferases generally have SET domains, which contain the catalytically critical residues identified in similar methyltransferases from other organisms [43]. Specifically, the alignment in **Fig. 2B** shows that the highly conserved catalytic tyrosine residue and the NHS motif involved in binding S-adenosine methionine are present within the SET domain [30]. These critical features are

absent from Chlamydomonas RMT2, although there is a tyrosine residue in the Chlamydomonas protein that is 9 amino acids upstream of the tyrosine conserved in other organisms.

Since the level of transcripts from the PSI genes are not strongly impacted in *rmt2* (**Fig. S4**), and the mutant doesn't appear to be affected in the turnover rate of PSI subunits (**Fig. S6**), the RMT2 protein is likely either directly or indirectly involved in translational or post-translational regulation of PSI biogenesis. Previous work showed that several photosynthetic processes are modulated by post-translational modifications; these processes include state transitions, the PSII repair cycle, control of translation through feedback control of CES proteins [44–46], and carbon assimilation [24]. With respect to PSI biogenesis, little is known about the role of PTMs, although PSI subunits appear to be methylated based on our data (**Table S3**). In this study we found that protein subunits of other photosynthetic complexes of Chlamydomonas are also methylated (**Table S3**). Despite the widespread occurrence of methylation on chloroplast proteins of Chlamydomonas, there is little known about the specific catalytic proteins involved in methylating these proteins or the functional consequence of this modification, which may cause conformation changes that alter biophysical and biochemical properties of the complexes [47]. One of the previously characterized putative methyltransferases in Chlamydomonas is CIA6, which is important for pyrenoid formation [48]. However, methyltransferase activity of CIA6 has not been confirmed, nor has its substrate been identified. Based on the use of fluorescently labeled fusion proteins, RMT2 appears to localize to the chloroplast and is potentially enriched in the pyrenoid. Importantly, *rmt2* mutants can still form pyrenoids (**Fig. 6B**) whereas *cia6* mutants cannot [48]. These results suggest that while CIA6 and RMT2 may both have functions in methylation of proteins, their downstream targets and their molecular roles appear to be functionally distinct. Furthermore, we identified Cre08.g378250, which encodes another methyltransferase that is required for the cells to remain protected under oxic conditions, although its location in the cell is not known. An additional methyltransferase, SMM7, was shown by others to be potentially pyrenoid localized [2].

The WT RMT2 protein fused to mNeonGreen was able to rescue the PSI deficient phenotype of the *rmt2* mutant, with the introduced fusion protein localized to the chloroplast with a strong signal associated with the pyrenoid (**Fig. 6**). The mutant also exhibited elevated accumulation of

the PSI assembly factors Ycf3 and Ycf4 (**Fig. 4**). The pyrenoid is an organelle specifically found in algae and hornworts and is important for CCM function [49,50]. It is traversed by thylakoid membrane tubules that penetrate the Rubisco matrix and is surrounded by a peripheral starch sheath [51]. Chloroplast stromal localized thylakoids perform photosynthetic electron transport and $O_2$ evolution, which would result in an oxic stroma that can generate ROS [52]. A study performed over 30 years ago suggested that pyrenoids contain active PSI but not PSII [53], with more recent studies showing that this plastid structure harbors several PSI subunits, but only a single PSII subunit [54]. Furthermore, recent spatial-interactome results demonstrated enrichment of PSI subunits in the pyrenoid while PSII subunits of the pyrenoid were only partially assembled or inactive [23,50]. Furthermore, the pyrenoid is separated from the rest of the stroma by a barrier that is likely to limit $O_2$ permeability. ROS generated in HL or conditions of nutrient deprivation may trigger changes in gene expression that are responsible for altering the pyrenoid structure and further physically isolating it from $O_2$. A peripheral pyrenoid mesh may enhance its physical compartmentalization and create the 'cement' that holds the starch plates in place, which may allow it to serve as a more effective diffusion barrier [55–57]. Additionally, recent proteomic work found that proteins involved in chloroplast translation may have physical associations with the pyrenoids [54,58].

Recently it was discovered that despite the presence of high external $CO_2$ (5 mM bicarbonate), treatment of Chlamydomonas with $H_2O_2$, which acts as a ROS signaling molecule [59], significantly increases the pyrenoid size, Rubisco relocation to the pyrenoid, and the formation of tight, thick starch plates that are held together by a peripheral mesh [55]. Aspects of the biogenesis of photosynthetic complexes can be susceptible to ROS damage, especially if Fe-S complexes are integral to their function. Therefore, we speculate that the pyrenoid may be a hypoxic micro-compartment serving as a site for the biogenesis of photosynthetic complexes. Therefore, the pyrenoid may not only provide protection from photorespiratory carbon metabolism catalyzed by Rubisco, but also function to protect $O_2$ sensitive processes such as PSI assembly [11,13]. These results are also congruent with RMT2 being enriched in the pyrenoid where it may interact with PSI assembly factors, and also with the *rmt2* mutants accumulating increased levels of the Ycf3

and Ycf4 PS1 assembly factors (**Fig. 4**). Previously, PSBP4, another PSI assembly factor, was shown to localize to thylakoid lumen puncta in the stroma and around the pyrenoids [23,60].

Taken together, our high-throughput $O_2$ sensitivity screen led to the discovery of the novel protein RMT2, which may be involved in post-translational modifications of proteins in the pyrenoid that are required for normal accumulation of PSI. The work provides new insight into the potential role of pyrenoids for compartmentation of $O_2$-sensitive processes such as PSI assembly. To understand RMT2 function, it is critical to identify the role of RMT2 in the assembly process and to determine if it has an activity associated with protein methylation. It is also important to obtain biochemical results that define the protein interaction network of RMT2, if that network is enriched in the pyrenoid, and how it might integrate into assembly processes associated with photosynthetic complexes.

## Materials and methods

### Strains and culture conditions

CMJ030 (CC-5325) was used as the WT strain for all experiments. Mutants in this study include *rmt2-1* (LMJ.RY0402.237082) and *rmt2-2* (LMJ.RY0402.255338), strains present in the CLiP mutant library (https://www.chlamylibrary.org/). Cells were grown in Tris Acetate Phosphate (TAP) solid and liquid medium. For photoautotrophic growth, Tris Phosphate (TP) medium (no acetate) was used. For all experiments, unless otherwise noted, strains were grown in constant LL (30 µmol photons $m^{-2}$ $s^{-1}$) and aerated by shaking. For growth under hypoxic conditions, cells were bubbled with a gas mixture (10% house air; 89.96% $N_2$; 0.04% $CO_2$) with constant stirring at 350 rpm at the indicated light intensities.

### Pooled mutant library screen

Chlamydomonas mutants from the CLiP library were collected after growth on agar plates and combined to generate a master pool of the entire library, as previously described [18,61]. Four aliquots of the master pool were inoculated into four cultures of 1 L of TAP medium to a final density of 20,000 cells $mL^{-1}$. The four cultures were grown under four different conditions: low

light hypoxic (LL-Hy), low light oxic (LL-Ox), high light hypoxic (HL-Hy), and high light oxic (HL-Ox). Growth was maintained for each of the cultures until the cell density reached approximately 2.5 million cells $mL^{-1}$ (7 doublings on average). Following the various treatments, total genomic DNA was extracted and isolated from the cells and used to amplify the unique barcodes associated with individual mutants; the amplification products were sequenced to quantify the level of each mutant in the culture.

**Analysis of oxygen sensitivity screen**

Based on barcode sequencing results from 3 replicates for each of the experimental treatments, each barcode in the sample was assigned read counts. Several criteria were sequentially applied to filter the initial counts. Insertions must be in 5' UTR, CDS, or intron regions of the gene; the insertion confidence level, defined in the initial analysis of the CLiP library and recorded in the description of each mutant (https://www.chlamylibrary.org/allMutants), must be 4 or better (from 53% to 95% confidence); the mean of the initial counts from the three replicates and from the final oxic HL and hypoxic HL conditions both were required to be greater than 10; 2 or more mutant alleles per gene were required for the mutants to be further considered. For the purposes of displaying the fold-change in abundance in cells transferred from oxic to hypoxic conditions (Hy/Ox ratio), the read counts of each specific gene were averaged for hypoxic conditions and then divided by the average for oxic conditions. The Hy/Ox ratios were interpreted as a quantification of the average differential fitness of each mutant associated with a specific mutant allele, under hypoxic compared to oxic conditions. The p-value of the read counts was calculated using a parametric bootstrap and modeled as Poisson counts.

**P700 activity measurements**

Absorbance changes associated with P700 oxidation and reduction were monitored at 705 nm and 740 nm using a JTS-100 spectrophotometer (SpectroLogiX, TN). Cells were pelleted by centrifugation and resuspended to a concentration of 30 µg chl $mL^{-1}$ in 20 mM HEPES-KOH, pH 7.2 and 10% ficoll. The suspension was made 10 µM DCMU to inhibit LEF prior to the measurement. Dark-adapted cells were exposed to 165 µmol photons $m^{-2}$ $s^{-1}$ during PSI oxidation followed by a saturating pulse as described in previous studies [11].

**$^{15}$N-labeling procedures for Chlamydomonas**

Single colonies (either the WT, *rmt2-1* or *rmt2-2* mutant cells) on TAP agar plates were inoculated in 5 mL of $^{15}$N-TAP medium, in which $^{14}NH_4Cl$, the sole nitrogen source, was replaced with $^{15}NH_4Cl$. After 5 d of growth in TAP, LL oxic conditions, the cells were diluted 100-fold in 50 mL of fresh $^{15}$N-TAP medium and then allowed to grow under appropriate conditions for the remainder of the experiment (2 additional days). For reciprocal labeling of mutant and WT cells, we performed the experiment identically, but the cells were labeled with $^{14}$N-TAP.

**Protein extraction and SDS-PAGE**

Cultures containing 30 µg of chl were collected by centrifugation at 3000 x *g* for 5 min and lysed and solubilized by adding 1X SDS-sample buffer (Cat. #1610737; Bio-Rad), heating the sample at 95 °C for 2 min and then centrifuging it for 5 min to pellet the cell debris. 10 µL of the supernatant containing approximately 3 µg of chl of a $^{14}$N-labeled sample was mixed with 10 µL of the supernatant containing the same amount of a $^{15}$N-labeled sample. Thus, 20 µL mixture of $^{14}$N- and $^{15}$N-labled samples was loaded onto a Tris-glycine 4-20% polyacrylamide gel (Mini-PROTEAN TGX; Bio-Rad) and the proteins of the sample separated by electrophoresis at 60 V for 1 h. The reciprocal labeling experiment was also performed.

**Complementation of *rmt2* mutants**

The pRam118 plasmid with VENUS [62] was used for complementation of the *rmt2* mutant strains. For the generation of the plasmid pRam118-RMT2-VENUS, genomic DNA for *RMT2* with an extended 5'UTR was assembled into the pRam118_VENUS plasmid using Gibson assembly [63]. The mutant strain *rmt2-2* was transformed with the plasmid pRam118-RMT2-VENUS and transformants screened for VENUS fluorescence as previously described [62]; transgenic cell lines were screened for VENUS fluorescence using a microplate reader (Infinite M1000; TECAN). Excitation and emission settings were, Venus, excitation 515/12 nm and emission 550/12 nm.

**Subcellular Localization of RMT2**

The pJM43-ble plasmid, which contains the gene encoding Bleomycin resistance, with a mNeonGreen tag from pYF015, was used for expression of *RMT2* [18]. For the generation of the pJM43-ble-RMT2-mNeonGreen construct expressing the *RMT2* gene, genomic *RMT2* DNA with the endogenous promoter and complete 5'UTR was assembled with the pJM43-ble-mNeonGreen plasmid using Gibson assembly [63]. The *rmt2-2* mutant was transformed with plasmid pJM43-ble-RMT2-mNeonGreen, transformants were selected for bleomycin resistance and then screened for mNeonGreen fluorescence as described [62]. Briefly, putative transgenic cells placed in individual wells of a microtiter plate were screened for mNeonGreen fluorescence using a microplate reader (Infinite M1000; TECAN). Excitation and emission settings were, mNeonGreen, excitation 488/12 nm and emission 520/5 nm. The strains that exhibited mNeonGreen fluorescence were used to localize the RMT2-mNeonGreen fusion protein using the TCS SP8 confocal laser-scanning microscope (Leica); excitation/emission settings were 488 nm/515-530 nm using the HyD SMD hybrid detector for mNeonGreen, and 488 nm/650-700 using the nm-HyD SMD hybrid detector for chl autofluorescence.

**PSI Turnover**

CMJ030, *rmt2-2* and *rmt2-2* (RMT2-mNG) cells were grown in TAP medium to log phase. The cultures were then centrifuged at 3000 x *g* for 5 min and the cell pellet was resuspended to 5 µg Chl $mL^{-1}$. 100 mL of cell suspension was transferred to two 250 mL Erlenmeyer flasks and one flask of each strain was treated simultaneously with chloramphenicol (250 µg $mL^{-1}$) and cycloheximide (10 µg $mL^{-1}$), which inhibit translation on 70S and 80S ribosomes, respectively. Cells of control and treated samples were harvested after 0, 6 and 24 hours and proteins were extracted as described above.

**In-gel digestion for LC/MS-MS**

Proteins were resolved by SDS-PAGE and different regions of the gel (based on molecular mass) were excised, diced into small pieces (1 $mm^2$), and placed into 0.65 mL tubes. The pieces were washed 3X by adding 200 µL of 25 mM ammonium bicarbonate/50% acetonitrile (ACN) followed by vortexing the suspension for 10 min, collecting the supernatant, and reducing and alkylating

the cysteine residues of the proteins present in the supernatant with 10 mM dithiothreitol (DTT) and 50 mM iodoacetamide (IAM), respectively; DTT was added to the sample, the sample incubated at 56 °C for 1 h and then made 50 mM IAM and incubated at room temperature for 45 min. The gel pieces were then washed with 25% ammonium bicarbonate/50% ACN, dried completely in a Speed Vac and treated with trypsin (5 ng $mL^{-1}$) at 37 °C overnight. The peptides were extracted three times from the gel pieces by adding 100 µL of 0.1% formic acid/50% ACN. The extracted peptides were dried in a Speed Vac, resuspended in 0.1% formic acid and then cleaned using a ziptip (Milipore ZipTips C18).

## Acknowledgments

RGK and JF were supported by the Department of Plant Biology of the Carnegie Institution for Science. WH was supported by the Department of Energy (DOE) Grant DE-SC0019417 (to ARG). PR was supported by Human Frontier of Science Program (HFSP) RGP0046/2018 (to ARG). FB was supported by the National Science Foundation (NSF) grant 1921429 (to ARG and Devaki Bhaya). RS was supported by the National Institutes of Health grant R01GM135706 (to S-LX). Andrey Malkovsky provided help with the microscope while Ruben Shrestha was a major contributor to the mass-spec analysis. We gratefully acknowledge the contribution of the Carnegie MS facility.

## References

1. Tardif, M. *et al.* PredAlgo: a new subcellular localization prediction tool dedicated to green algae. *Mol. Biol. Evol.* **29**, 3625–3639 (2012).
2. Wang, L. *et al.* A chloroplast protein atlas reveals punctate structures and spatial organization of biosynthetic pathways. *Cell* **186**, 3499–3518.e14 (2023).
3. Chitnis, P. R. PHOTOSYSTEM I: Function and Physiology. *Annu. Rev. Plant Physiol. Plant Mol. Biol.* **52**, 593–626 (2001).
4. Busch, A. & Hippler, M. The structure and function of eukaryotic photosystem I. *Biochim. Biophys. Acta* **1807**, 864–877 (2011).
5. Amunts, A., Drory, O. & Nelson, N. The structure of a plant photosystem I supercomplex at 3.4 A resolution. *Nature* **447**, 58–63 (2007).
6. Jordan, P. *et al.* Three-dimensional structure of cyanobacterial photosystem I at 2.5 A resolution. *Nature* **411**, 909–917 (2001).
7. Malavath, T., Caspy, I., Netzer-El, S. Y., Klaiman, D. & Nelson, N. Structure and function of wild-type and subunit-depleted photosystem I in Synechocystis. *Biochimica et Biophysica Acta (BBA) - Bioenergetics* **1859**, 645–654 (2018).
8. Mazor, Y., Nataf, D., Toporik, H. & Nelson, N. Crystal structures of virus-like photosystem I complexes from the mesophilic cyanobacterium Synechocystis PCC 6803. *Elife* **3**, e01496 (2013).
9. Schöttler, M. A., Albus, C. A. & Bock, R. Photosystem I: its biogenesis and function in higher plants. *J. Plant Physiol.* **168**, 1452–1461 (2011).

10. Yang, H., Liu, J., Wen, X. & Lu, C. Molecular mechanism of photosystem I assembly in oxygenic organisms. *Biochim. Biophys. Acta* **1847**, 838–848 (2015).
11. Heinnickel, M. *et al.* Tetratricopeptide repeat protein protects photosystem I from oxidative disruption during assembly. *Proc. Natl. Acad. Sci. U. S. A.* **113**, 2774–2779 (2016).
12. Nellaepalli, S., Ozawa, S.-I., Kuroda, H. & Takahashi, Y. The photosystem I assembly apparatus consisting of Ycf3-Y3IP1 and Ycf4 modules. *Nat. Commun.* **9**, 2439 (2018).
13. Nellaepalli, S., Kim, R. G., Grossman, A. R. & Takahashi, Y. Interplay of four auxiliary factors is required for the assembly of photosystem I reaction center subcomplex. *Plant J.* **106**, 1075–1086 (2021).
14. Ozawa, S.-I., Onishi, T. & Takahashi, Y. Identification and characterization of an assembly intermediate subcomplex of photosystem I in the green alga Chlamydomonas reinhardtii. *J. Biol. Chem.* **285**, 20072–20079 (2010).
15. Imlay, J. A. Iron-sulphur clusters and the problem with oxygen. *Mol. Microbiol.* **59**, 1073–1082 (2006).
16. Bruska, M. K., Stiebritz, M. T. & Reiher, M. Analysis of differences in oxygen sensitivity of Fe-S clusters. *Dalton Trans.* **42**, 8729–8735 (2013).
17. Lang, S. M., Barnett, R. N. & Landman, U. Oxygen Sensitivity of Free Nonligated Iron–Sulfur Clusters. *J. Phys. Chem. C* **123**, 27681–27689 (2019).
18. Li, X. *et al.* A genome-wide algal mutant library and functional screen identifies genes required for eukaryotic photosynthesis. *Nat. Genet.* **51**, 627–635 (2019).
19. Fauser, F. *et al.* Systematic characterization of gene function in the photosynthetic alga Chlamydomonas reinhardtii. *Nat. Genet.* **54**, 705–714 (2022).

20. Serre, N. B. C., Alban, C., Bourguignon, J. & Ravanel, S. An outlook on lysine methylation of non-histone proteins in plants. *J. Exp. Bot.* **69**, 4569–4581 (2018).

21. Murn, J. & Shi, Y. The winding path of protein methylation research: milestones and new frontiers. *Nat. Rev. Mol. Cell Biol.* **18**, 517–527 (2017).

22. Udeshi, N. D., Mertins, P., Svinkina, T. & Carr, S. A. Large-scale identification of ubiquitination sites by mass spectrometry. *Nat. Protoc.* **8**, 1950–1960 (2013).

23. Mackinder, L. C. M. *et al.* A Spatial Interactome Reveals the Protein Organization of the Algal CO2-Concentrating Mechanism. *Cell* **171**, 133–147.e14 (2017).

24. Grabsztunowicz, M., Koskela, M. M. & Mulo, P. Post-translational Modifications in Regulation of Chloroplast Function: Recent Advances. *Front. Plant Sci.* **8**, 240 (2017).

25. Lehtimäki, N., Koskela, M. M. & Mulo, P. Posttranslational Modifications of Chloroplast Proteins: An Emerging Field. *Plant Physiol.* **168**, 768–775 (2015).

26. Hippler, M., Biehler, K., Krieger-Liszkay, A., van Dillewjin, J. & Rochaix, J. D. Limitation in electron transfer in photosystem I donor side mutants of Chlamydomonas reinhardtii. Lethal photo-oxidative damage in high light is overcome in a suppressor strain deficient in the assembly of the light harvesting complex. *J. Biol. Chem.* **275**, 5852–5859 (2000).

27. Fischer, N., Sétif, P. & Rochaix, J. D. Targeted mutations in the psaC gene of Chlamydomonas reinhardtii: preferential reduction of FB at low temperature is not accompanied by altered electron flow from photosystem I to ferredoxin. *Biochemistry* **36**, 93–102 (1997).

28. Karpowicz, S. J., Prochnik, S. E., Grossman, A. R. & Merchant, S. S. The GreenCut2 resource, a phylogenomically derived inventory of proteins specific to the plant lineage. *J. Biol.*

*Chem.* **286**, 21427–21439 (2011).

29. Dillon, S. C., Zhang, X., Trievel, R. C. & Cheng, X. The SET-domain protein superfamily: protein lysine methyltransferases. *Genome Biol.* **6**, 227 (2005).
30. Wilkinson, A. W. *et al.* SETD3 is an actin histidine methyltransferase that prevents primary dystocia. *Nature* **565**, 372–376 (2019).
31. Wakao, S. *et al.* Discovery of photosynthesis genes through whole-genome sequencing of acetate-requiring mutants of Chlamydomonas reinhardtii. *PLoS Genet.* **17**, e1009725 (2021).
32. Rochaix, J., Fischer, N. & Hippler, M. Chloroplast site-directed mutagenesis of photosystem I in Chlamydomonas: electron transfer reactions and light sensitivity. *Biochimie* **82**, 635–645 (2000).
33. Sommer, F., Hippler, M., Biehler, K., Fischer, N. & Rochaix, J.-D. Comparative analysis of photosensitivity in photosystem I donor and acceptor side mutants of Chlamydomonas reinhardtii. *Plant Cell Environ.* **26**, 1881–1892 (2003).
34. Dmitrieva, V. A., Tyutereva, E. V. & Voitsekhovskaja, O. V. Singlet Oxygen in Plants: Generation, Detection, and Signaling Roles. *Int. J. Mol. Sci.* **21**, (2020).
35. Khorobrykh, S., Havurinne, V., Mattila, H. & Tyystjärvi, E. Oxygen and ROS in Photosynthesis. *Plants* **9**, (2020).
36. Houtz, R. L., Stults, J. T., Mulligan, R. M. & Tolbert, N. E. Post-translational modifications in the large subunit of ribulose bisphosphate carboxylase/oxygenase. *Proc. Natl. Acad. Sci. U. S. A.* **86**, 1855–1859 (1989).
37. Ma, S. *et al.* Molecular Evolution of the Substrate Specificity of Chloroplastic

Aldolases/Rubisco Lysine Methyltransferases in Plants. *Mol. Plant* **9**, 569–581 (2016).

38. Houtz, R. L., Royer, M. & Salvucci, M. E. Partial Purification and Characterization of Ribulose-1,5-bisphosphate Carboxylase/Oxygenase Large Subunit epsilonN-Methyltransferase. *Plant Physiol.* **97**, 913–920 (1991).
39. Wang, P., Royer, M. & Houtz, R. L. Affinity purification of ribulose-1,5-bisphosphate carboxylase/oxygenase large subunit epsilon N-methyltransferase. *Protein Expr. Purif.* **6**, 528–536 (1995).
40. Klein, R. R. & Houtz, R. L. Cloning and developmental expression of pea ribulose-1,5-bisphosphate carboxylase/oxygenase large subunit N-methyltransferase. *Plant Mol. Biol.* **27**, 249–261 (1995).
41. Ying, Z., Mulligan, R. M., Janney, N. & Houtz, R. L. Rubisco small and large subunit N-methyltransferases. Bi- and mono-functional methyltransferases that methylate the small and large subunits of Rubisco. *J. Biol. Chem.* **274**, 36750–36756 (1999).
42. Alban, C. *et al.* Uncovering the protein lysine and arginine methylation network in Arabidopsis chloroplasts. *PLoS One* **9**, e95512 (2014).
43. Trievel, R. C., Flynn, E. M., Houtz, R. L. & Hurley, J. H. Mechanism of multiple lysine methylation by the SET domain enzyme Rubisco LSMT. *Nat. Struct. Biol.* **10**, 545–552 (2003).
44. Depège, N., Bellafiore, S. & Rochaix, J.-D. Role of chloroplast protein kinase Stt7 in LHCII phosphorylation and state transition in Chlamydomonas. *Science* **299**, 1572–1575 (2003).
45. Aro, E. M., Virgin, I. & Andersson, B. Photoinhibition of Photosystem II. Inactivation, protein damage and turnover. *Biochim. Biophys. Acta* **1143**, 113–134 (1993).

46. Choquet, Y. *et al.* Translation of cytochrome f is autoregulated through the 5' untranslated region of petA mRNA in Chlamydomonas chloroplasts. *Proc. Natl. Acad. Sci. U. S. A.* **95**, 4380–4385 (1998).

47. Luo, M. Chemical and Biochemical Perspectives of Protein Lysine Methylation. *Chem. Rev.* **118**, 6656–6705 (2018).

48. Ma, Y., Pollock, S. V., Xiao, Y., Cunnusamy, K. & Moroney, J. V. Identification of a novel gene, CIA6, required for normal pyrenoid formation in Chlamydomonas reinhardtii. *Plant Physiol.* **156**, 884–896 (2011).

49. Wang, L. & Jonikas, M. C. The pyrenoid. *Curr. Biol.* **30**, R456–R458 (2020).

50. Barrett, J., Girr, P. & Mackinder, L. C. M. Pyrenoids: CO2-fixing phase separated liquid organelles. *Biochim. Biophys. Acta Mol. Cell Res.* **1868**, 118949 (2021).

51. Meyer, M. T. *et al.* Assembly of the algal $CO_2$-fixing organelle, the pyrenoid, is guided by a Rubisco-binding motif. *Science Advances* **6**, eabd2408 (2020).

52. Roach, T., Na, C. S. & Krieger-Liszkay, A. High light-induced hydrogen peroxide production in Chlamydomonas reinhardtii is increased by high CO2 availability. *Plant J.* **81**, 759–766 (2015).

53. McKay, R. M. L. & Gibbs, S. P. Composition and function of pyrenoids: cytochemical and immunocytochemical approaches. *Can. J. Bot.* **69**, 1040–1052 (1991).

54. Zhan, Y. *et al.* Pyrenoid functions revealed by proteomics in Chlamydomonas reinhardtii. *PLoS One* **13**, e0185039 (2018).

55. Neofotis, P. *et al.* The Induction of Pyrenoid Synthesis by Hyperoxia and its Implications for the Natural Diversity of Photosynthetic Responses in Chlamydomonas. *bioRxiv*

2021.03.10.434646 (2021) doi:10.1101/2021.03.10.434646.

56. Fei, C., Wilson, A. T., Mangan, N. M., Wingreen, N. S. & Jonikas, M. C. Diffusion barriers and adaptive carbon uptake strategies enhance the modeled performance of the algal CO2-concentrating mechanism. *bioRxiv* 2021.03.04.433933 (2021) doi:10.1101/2021.03.04.433933.

57. Toyokawa, C., Yamano, T. & Fukuzawa, H. Pyrenoid Starch Sheath Is Required for LCIB Localization and the CO2-Concentrating Mechanism in Green Algae1 [OPEN]. *Plant Physiol.* **182**, 1883–1893 (2020).

58. Sun, Y. *et al.* Photosystem Biogenesis Is Localized to the Translation Zone in the Chloroplast of Chlamydomonas. *Plant Cell* **31**, 3057–3072 (2019).

59. Foyer, C. H. Reactive oxygen species, oxidative signaling and the regulation of photosynthesis. *Environ. Exp. Bot.* **154**, 134–142 (2018).

60. Liu, J. *et al.* PsbP-domain protein1, a nuclear-encoded thylakoid lumenal protein, is essential for photosystem I assembly in Arabidopsis. *Plant Cell* **24**, 4992–5006 (2012).

61. Vilarrasa-Blasi, J. *et al.* Systematic characterization of gene function in a photosynthetic organism. *bioRxiv* 2020.12.11.420950 (2020) doi:10.1101/2020.12.11.420950.

62. Kaye, Y. *et al.* The mitochondrial alternative oxidase from *Chlamydomonas reinhardtii* enables survival in high light. *J. Biol. Chem.* **294**, 1380–1395 (2019).

63. Gibson, D. G. *et al.* Enzymatic assembly of DNA molecules up to several hundred kilobases. *Nat. Methods* **6**, 343–345 (2009).